Eur. Phys. J. Appl. Phys. (2013) 63: 30401
DOI: 10.1051/epjap/2013130257

THE EUROPEAN PHYSICAL JOURNAL APPLIED PHYSICS

Regular Article

Highly crystalline core-shell FeCo-$CoFe_2O_4$ nanostructures

Brigitte Paterson[1,2], Parshu Gyawali[2], David McKeown[2], Andrew Buechele[2], Ian L. Pegg[1,2], and John Philip[1,2,a]

[1] Department of Physics, The Catholic University of America, Washington, DC 20064, USA
[2] The Vitreous State Laboratory, The Catholic University of America, Washington, DC 20064, USA

Received: 28 May 2013 / Received in final form: 30 August 2013 / Accepted: 3 September 2013
Published online: 27 September 2013 –

Abstract. Highly crystalline core-shell FeCo-$CoFe_2O_4$ nanowires were obtained from a three step process. Initially, $CoFe_2O_4$ nanowires were grown using electrospinning and annealing at higher temperatures. Through a thermal reduction under controlled conditions, $CoFe_2O_4$ nanostructures were converted to FeCo alloy nanowires. Then by natural oxidation, a highly crystalline shell of $CoFe_2O_4$ formed over the FeCo core structure. Structural and magnetic characterizations revealed the presence of highly crystalline FeCo-Co_2FeO_4 core-shell structure. Magnetically, the soft FeCo phase switches at a lower magnetic field compared to the hard $CoFe_2O_4$ phase, yielding an irregular hysteresis loop with a squeezed loop in the middle. The FeCo/$CoFe_2O_4$ core-shell is stable and it retains its structure for a prolonged duration.

1 Introduction

Soft ferromagnetic materials, such as FeCo alloys, with high saturation magnetization, permeability and Curie temperature have been of great interest for applications in industry. At room temperature iron-rich cobalt alloys, with 30% cobalt content, have the highest saturation magnetization of all known materials [1]. These desirable magnetic properties of FeCo alloys are in high demand for use in spintronic devices [2], transformer cores, magnetoresistive devices [3] and as microwave absorption materials to combat interference pollution [4]. On the other hand, $CoFe_2O_4$ (CFO) is a ferromagnetic insulator and explored for many applications, including high temperature spin-filter applications [5]. It is highly desirable to fabricate core-shell FeCo-$CoFe_2O_4$ for several critical applications. Core-shell FeCo-CFO nanoparticles were reported with crystalline core and amorphous shell [6,7]. In this study, we have fabricated highly crystalline core-shell FeCo-CFO nanowires. We have carried out structural and magnetic characterization that revealed the highly crystalline nature of the core FeCo and the shell $CoFe_2O_4$.

Core-shell FeCo-$CoFe_2O_4$ structures were fabricated using a three step process. First, cobalt ferrite nanofibers were grown using the electrospinning process followed by annealing. After fabrication, these nanowires were subjected to additional heating schemes in order to convert them to FeCo (Fe_7Co_3) alloy nanowires. The resulting FeCo alloy nanostructures were chemically stable and retained their desirable magnetic properties over time. Magnetic measurements of the FeCo nanostructures showed that they were soft magnets at room temperature and at low temperature (10 K) with low coercivity and high saturation magnetization. They were allowed to oxidize naturally on the surface and crystalline core-shell FeCo-CFO nanowires were obtained.

2 Experimental details

High quality CFO nanowires with average diameters of 100 nm were grown by the electospinning process [8,9]. After the electrospinning process, the collected nanowires were annealed at 923 K for 2 h to evaporate the polymers, polyvinylpyrrolidone and polyvinyl alcohol in ultra-high purity argon and oxygen gas mixture. The samples were then annealed at 1003 K for 90 min in the same atmosphere to form the cobalt ferrite nanostructures. Well characterized CFO nanowires were thermally reduced in a hydrogen atmosphere. This reduction process involved heating samples in a quartz tube furnace at 923 K for 20 min in argon and hydrogen gas mixture.

The morphology of the nanowires was analyzed using a scanning electron microscope (SEM) (JEOL JSM-6300); the crystal structure was investigated by X-ray diffraction (XRD) (Thermo/ARL X'TRA, Cu-K_α); and Raman spectra were obtained using an in-house built Raman system with a 514.5 nm Ar^+ laser (Lexel Laser 3000). Magnetic measurements were carried-out using a vibrating sample magnetometer (VSM – quantum design). We will discuss the characterization of CFO nanowires first and then the conversion of CFO to FeCo, characterization of FeCo and the core-shell nanostructures.

[a] e-mail: philip@cua.edu

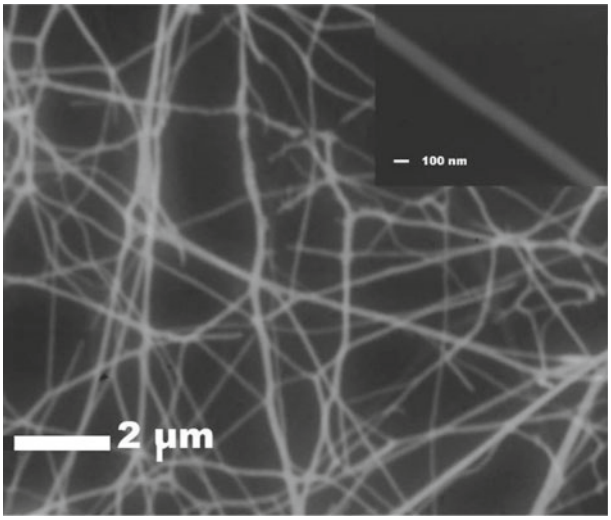

Fig. 1. SEM image of CFO nanowires obtained after electrospinning. Inset: single CFO nanowire with a diameter of 100 nm.

3 Results and discussion

3.1 Structural characterization

Figure 1 shows micrographs of CFO nanowires on silicon substrate. Electrospinning yields a random array of continuous nanowires having an average diameter of roughly 100 nm. These nanowires have lengths ranging from 50–100 μm. The X-ray diffraction pattern displayed in Figure 2a shows that the CFO nanowires have an inverse spinel structure [10–16]; the relative intensities of the diffraction peaks match those of the $CoFe_2O_4$ powder diffraction pattern (ICDD #01-071-5029). Room temperature Raman spectroscopy of the CFO nanowires in Figure 2b shows distinct peak maxima at 221, 300, 478, 624 and 698 cm^{-1}. The peaks at ∼300 cm^{-1} and 221, 478 cm^{-1} correspond to the E_g and T_{2g} modes, respectively. These low frequency phonon modes are due to symmetric and antisymmetric bending of metallic ion-oxygen bonds in the octahedral voids. The peaks at ∼624 cm^{-1} and ∼698 cm^{-1} are indicative of the A_{1g} symmetry and are due to metal cation-oxygen anion stretching in the tetrahedral sublattice [17–19].

3.2 Magnetic measurements of CFO nanowires

For the magnetic characterization, the external field was applied parallel to the substrate plane and the substrate background is corrected from all magnetic measurements. Figure 3a shows the magnetic hysteresis loop of the CFO nanowires at 300 and 10 K. From this, we can deduce that the nanowires display a coercivity of about $H_c = 1300$ Oe at 300 K. At 10 K, they exhibit hard ferrimagnetic behavior with an increased coercivity of $H_c = 8300$ Oe. The magnetization of CFO as a function of temperature was also investigated in this study. Magnetization of CFO with

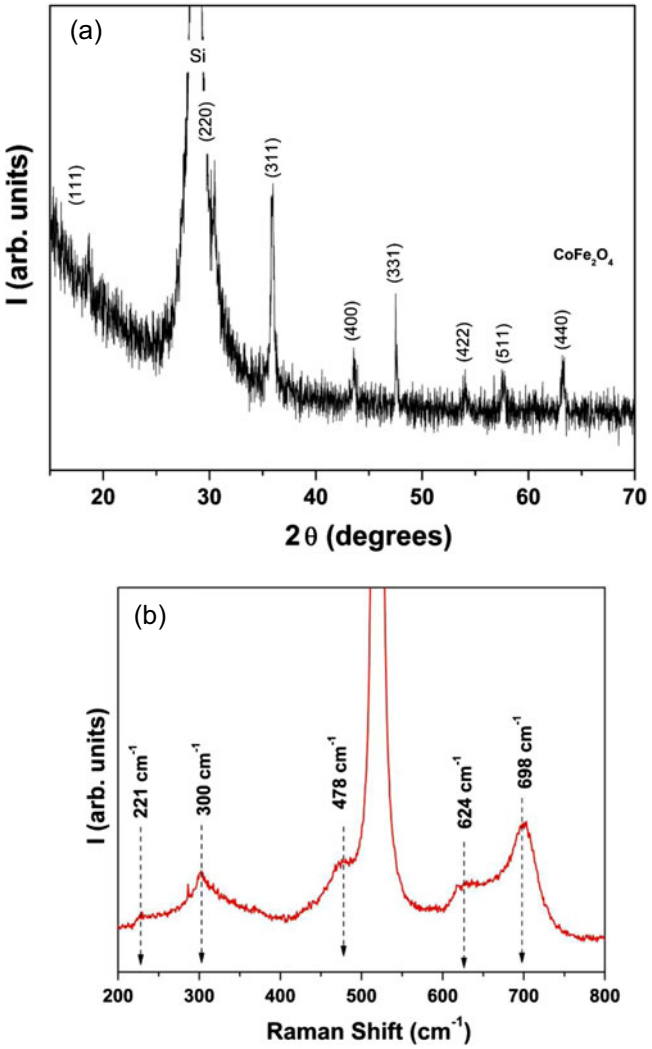

Fig. 2. (a) XRD pattern of CFO nanowires on silicon substrate. The peak from silicon substrate is also marked. (b) Raman spectrum of CFO nanowires deposited on silicon substrate. The peak from substrate appears around 520 cm^{-1}.

an external magnetic field ($H = 10,000$ Oe) applied parallel to the substrate is shown in Figure 3b. The CFO samples show a Curie temperature (T_c) of nearly 850 K. This is higher than the known T_c of bulk CFO, which is around 793 K [1]. Cation redistribution occurs between the tetrahedral and octahedral sublattices of CFO at temperatures above 973 K [20]. The annealing temperatures used during sample preparation of CFO nanowires could result in the movement of Co^{2+} and Fe^{3+} ions within the two sublattices. This temperature dependent redistribution could explain the increase of the Curie temperature of cobalt ferrite [21].

3.3 Conversion of CFO to FeCo nanowires

High quality CFO nanowires are annealed at 923 K in argon with 10% hydrogen atmosphere for 20 min and then cooled to room temperature in the same ambient.

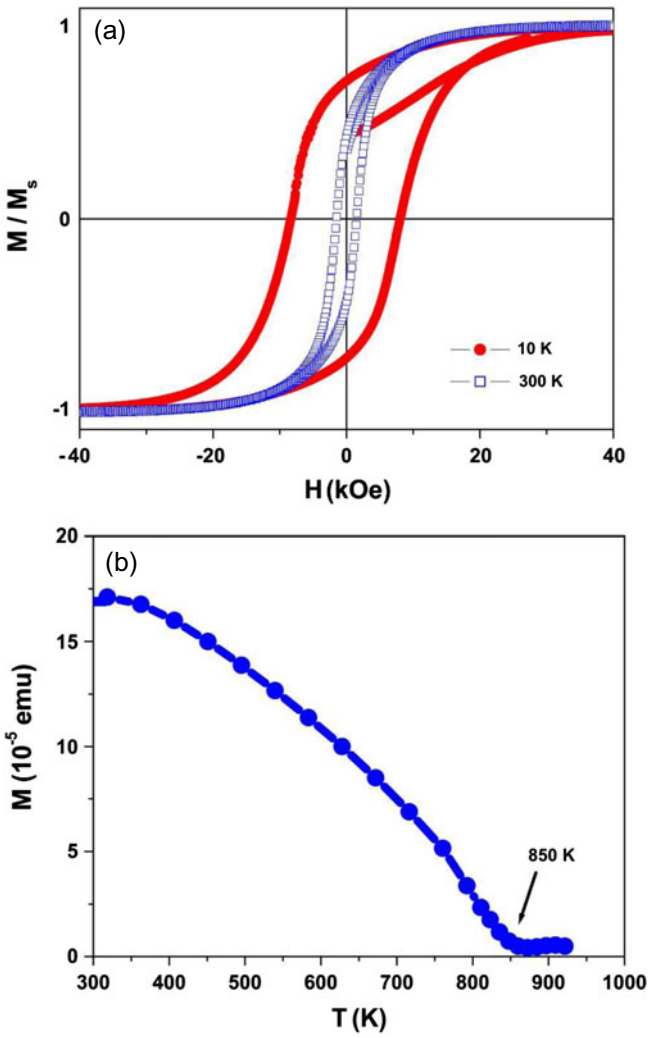

Fig. 3. (a) Hysteresis loop of $CoFe_2O_4$ nanowires at 300 K and 10 K (b) M vs. T plot of CFO showing that the Curie temperature is around 850 K.

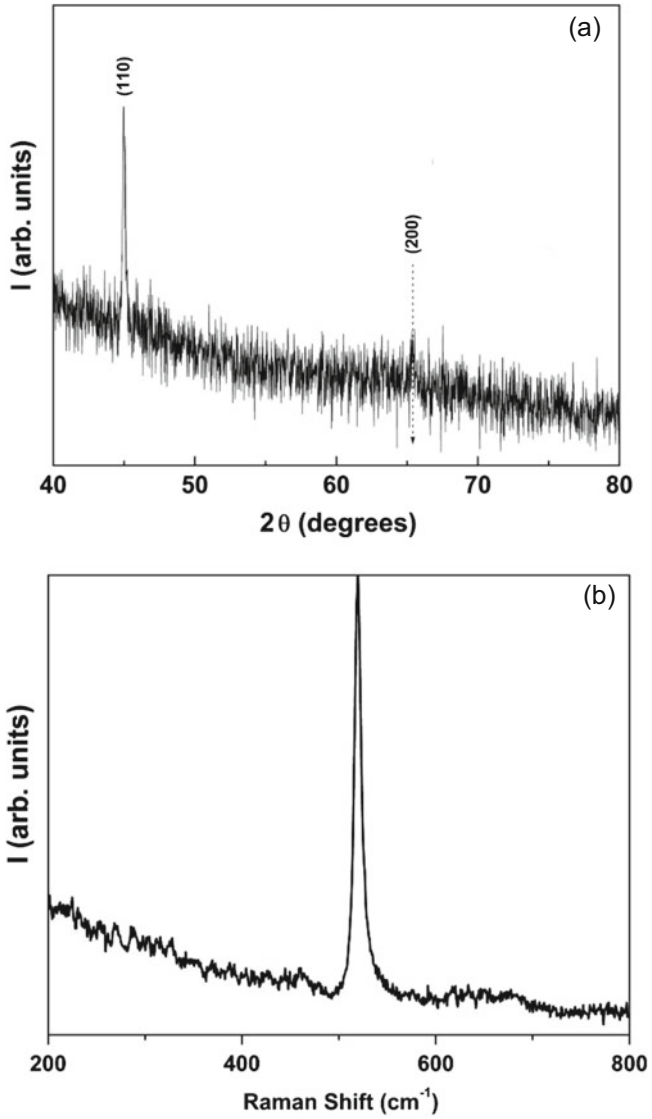

Fig. 4. (a) XRD pattern of FeCo alloy nanowires. Dashed line indicate the peak corresponding to *hkl* value (2 0 0). (b) Raman spectrum of FeCo alloy nanowires on silicon substrate.

After thermal reduction, the nanowires maintain their continuous and cylindrical shape. The SEM image appears similar to what is shown in Figure 1. The XRD analyses of the thermally reduced samples in Figure 4a show that these structures exhibit the BCC crystal structure of an intermetallic iron-cobalt (Fe_7Co_3) alloy [ICDD #00-49-1568]. The FeCo alloy nanowires have no Raman active modes because of the high level of symmetry of the BCC lattice of FeCo crystal structure (Fig. 4b). The Raman spectrum shown in Figure 4b displays only the peak from the substrate (silicon). Raman spectra along with the characteristic data from XRD indicate that the nanowires are initially CFO and then are reduced to become FeCo. In Figure 5a, the hysteresis loops for the FeCo alloy nanowires at room temperature and 10 K show low coercivity. The coercivity at 10 and 300 K are 58 and 54 Oe respectively. These properties are analogous to bulk FeCo [7]. FeCo alloys with 30%–50% cobalt composition have higher Curie temperatures than pure phase iron (1043 K) [1]. Figure 5b shows the magnetization $(M(T)/M_s)$ plotted over (T/T_c). The experimental data below T_c is fitted with a power law, $M(T) \sim (T_c - T)^{\beta}$ [22,23]. The T_c obtained from the fit is 1300 ± 40 K and the value of β is 0.33. The β value is typically between 0.33 and 0.37 for ferromagnets and ferrimagnets [23]. The T_c of FeCo nanowires obtained from the fit matches with the reported Curie temperature for FeCo alloys (1280 K) [22].

3.3.1 Formation of core-shell FeCo-$CoFe_2O_4$ nanostructures

FeCo nanostructures are naturally oxidized to form core-shell FeCo-$CoFe_2O_4$ nanowires. We have studied the CFO shell formation as a function of time. Figure 6a shows the XRD patterns after 1–4 weeks of natural oxidation. In the first two weeks, nanowires show the XRD pattern of FeCo structure with no detectable CFO shell. A CFO phase

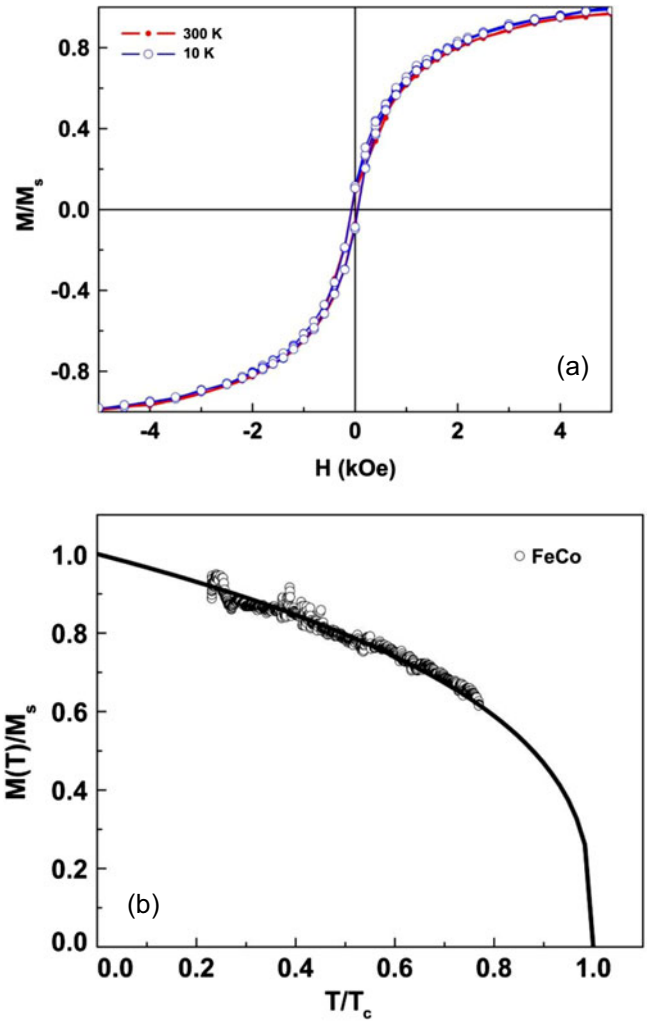

Fig. 5. (a) Hysteresis loops of FeCo alloy nanowires at 300 K and 10 K; (b) M vs. T plot of FeCo showing a T_c around 1300 K.

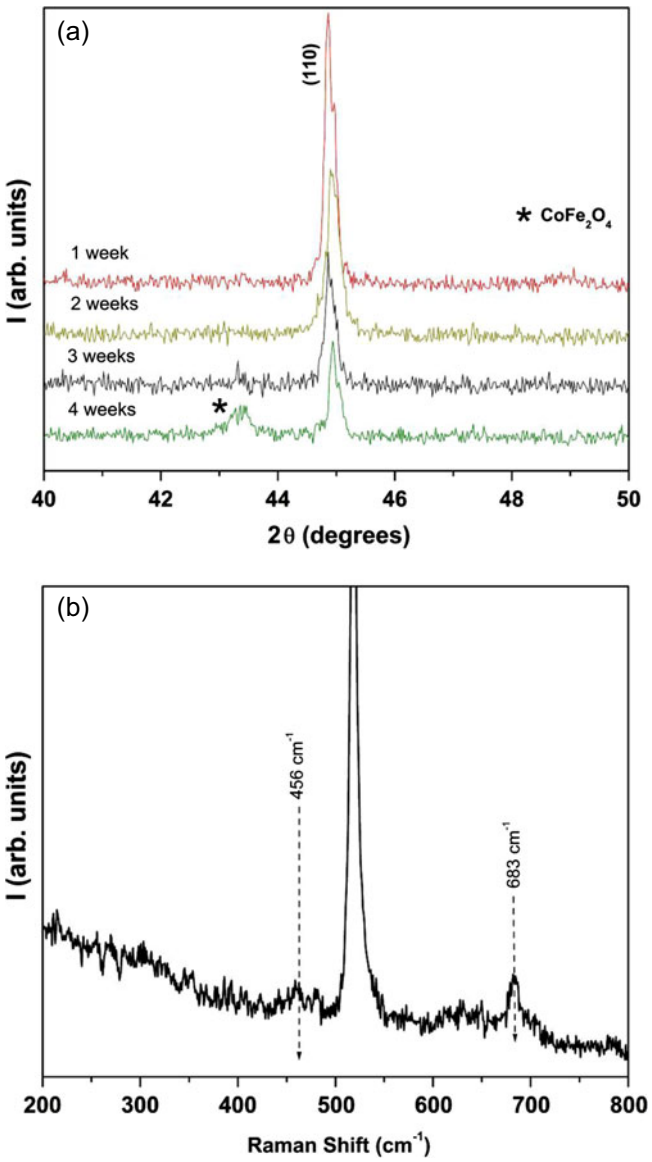

Fig. 6. (a) XRD patterns of FeCo nanowires after natural oxidation at different durations. The peak due to BCC FeCo is marked with *hkl* (1 1 0). The CFO peak emerges after nearly three weeks of exposure to air. (b) Raman spectrum of FeCo alloy nanowires after being exposed to air for one week. The peak around 520 cm^{-1} is due to silicon substrate.

emerged in the pattern after three weeks. Very thin formations of CFO on the surface of the FeCo nanowires are not detectable via XRD diffraction analyses. However, Raman analyses did show the presence of a small amount of CFO phase over the FeCo alloys after one week of exposure to air (Fig. 6b). The two Raman peaks observed are shifted to lower wavenumbers compared to the peaks in Figure 2b. This is due to the very thin CFO shell formed on the FeCo core [17]. The XRD results in Figure 6a suggest that the cobalt and iron are not forming individual oxides but that the entire surface of the nanostructure is oxidized to form a CFO phase. SEM micrographs of the core-shell do not provide any new information other than what is displayed in Figure 1. We have carried out high-resolution transmission electron microscopy (TEM) studies to understand the core-shell formation. FeCo nanowires that are exposed to air for two months are chosen for the TEM study. High-resolution TEM images show clear formation of a core-shell (Fig. 7a) structure. The radius of the core is around 25–30 nm and the shell has a thickness around 10 nm. The lattice fringes of the shell correspond to (1 1 1) planes of CFO. It is observed that the shell is polycrystalline in nature. Earlier studies on core-shell nanoparticles have shown a crystalline core of FeCo and an amorphous shell of CFO [6,7]. Our results are encouraging for fabricating a variety of devices that require crystalline core and shell. We have also carried out the M vs. H studies on core-shell nanostructures after two months of exposure to air (Fig. 7b). In the case of FeCo/CFO, FeCo is a soft magnet with very low coercivity and CFO is a ferrimagnet with high coercivity. There will be no magnetic exchange interaction between the ferromagnetic FeCo and ferromagnetic CFO if the dimension of the FeCo is larger than twice the domain wall width of the CFO [24]. As shown in the

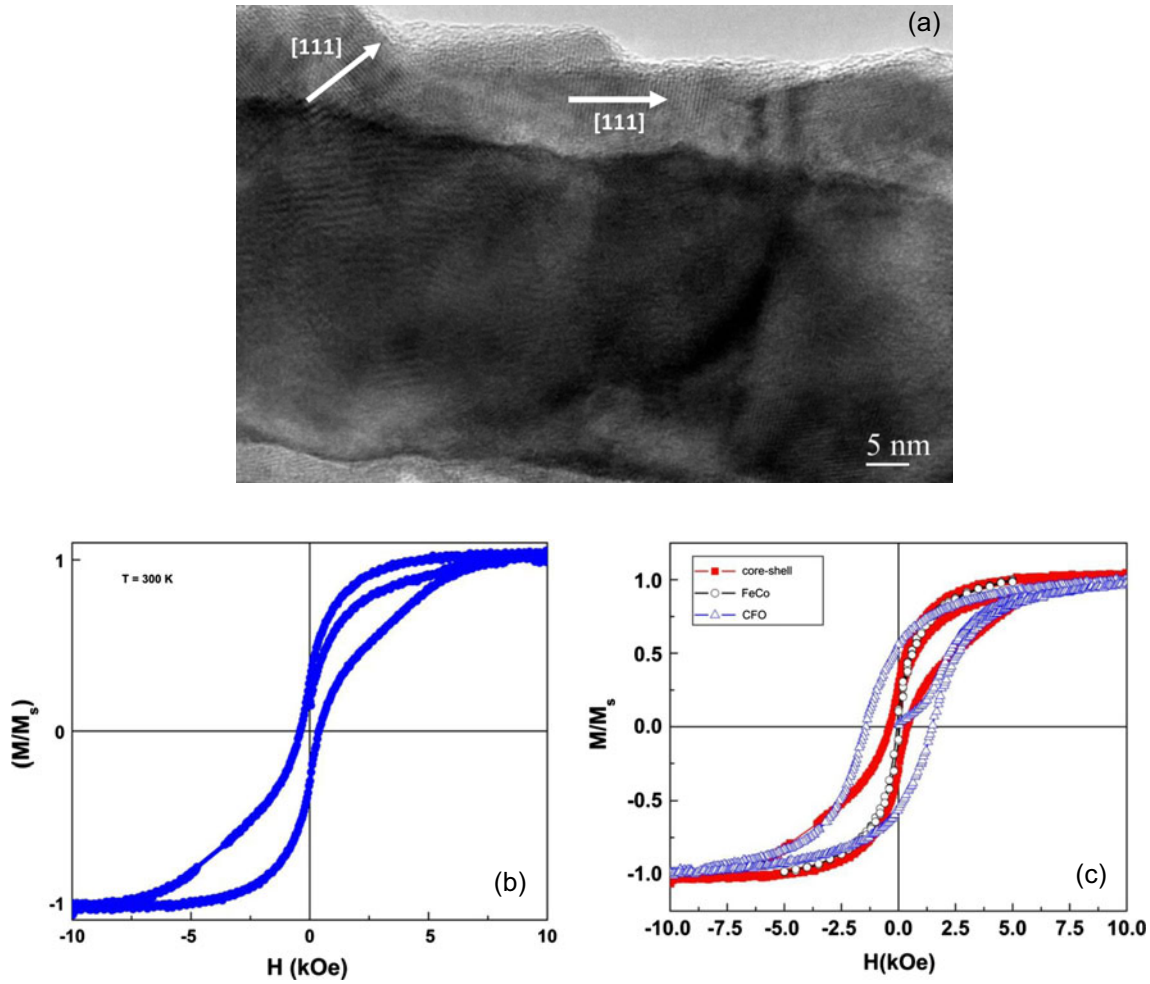

Fig. 7. (a) High-resolution TEM image of core-shell FeCo-CFO nanowire. The image shows that the core and the shell are crystalline. (b) M vs. H plot of core-shell FeCo-CFO after two months of natural oxidation. (c) The M-H curves of FeCo, CFO and core-shell nanostructures plotted together to understand the two-phase magnetic behavior of the core-shell structures.

TEM image, a large volume is occupied by the FeCo alloy. Therefore, in a core-shell structure with a large soft phase, core and shell structures are not able to switch cooperatively. As a result the hysteresis displays two-phase behavior (Fig. 7b). In Figure 7c, M-H curves of FeCo, CFO and the core-shell are plotted together to understand the two-phase magnetic behavior of the core-shell structure. The FeCo alloy switches at a lower field, so we observe an irregular shape with a narrow loop in the middle. The coercivity of the FeCo core appears slightly higher than the FeCo nanowire. This is because of the reduction in the diameter of the core due to CFO shell formation. Similar hysteresis loop is observed after 6 months of natural oxidation, indicating that the core-shell structure is stable over a long duration.

4 Conclusion

Core-shell FeCo-CFO nanowires are fabricated using a three step process. CFO nanowires are grown first and they are reduced to form FeCo, then by natural oxidation, a shell of CFO is formed over FeCo. It is observed that the core-shell structure is retained over a long period. The core (FeCo) as well as the shell (CFO) is highly crystalline. The crystalline nature of both the core FeCo and shell CFO makes it a suitable candidate for several novel applications. The hysteresis loop at higher temperature exhibits two-phase magnetic behavior.

This work was supported by National Science Foundation under ECCS-0845501 and NSF-MRI, DMR-0922997. We thank Cathy Paul for carefully reading the manuscript.

References

1. B.D. Cullity, *Introduction to Magnetic Materials* (IEEE Press, Piscatawny, NJ, 2009), p. 466
2. S. Anderson, V. Korenivsk, J. Appl. Phys. **107**, 09D711 (2010)
3. Y.H. Ren, C. Wu, Y. Gong, C. Pettiford, N.X. Sun, J. Appl. Phys. **105**, 073910 (2009)

4. R.C. Che, L.M. Peng, X.F. Duan, Q. Chen, X.L. Liang, Adv. Mater. **16**, 401 (2004)
5. A.V. Ramos, M.-J. Guittet, J.-B. Moussy, R. Mattana, C. Deranlot, F. Petroff, C. Gatel, Appl. Phys. Lett. **91**, 122107 (2007)
6. G.H. Jaffari, S.R. Ali, S.K. Hasanain, G. Güntherodt, S.I. Shah, J. Appl. Phys. **108**, 063921 (2010)
7. Y.X. Gong, L. Zhen, J.T. Jiang, C.Y. Xu, W.Z. Shao, J. Appl. Phys. **106**, 064302 (2009)
8. M. Sangmanee, S. Maensiri, Appl. Phys. A **97**, 167 (2009)
9. D. Li, J.T. McCann, Y. Xia, J. Am. Ceram. Soc. **89**, 1861 (2006)
10. G.A. Sawatzky, F. Van Der Woude, A.H. Morrish, J. Appl. Phys. **39**, 1204 (1968)
11. G.A. Sawatzky, F. Van Der Woude, A.H. Morrish, Phys. Rev. **187**, 747 (1969)
12. T.A.S. Ferreira, J.C. Waerenborgh, M.H.R.M. Mendonca, M.R. Nunes, F.M. Costa, Solid State Sci. **5**, 383 (2003)
13. P.J. Murray, J.W. Linnett, J. Phys. Chem. Solids **37**, 1041 (1976)
14. P.J. Murray, J.W. Linnett, J. Phys. Chem. Solids **37**, 619 (1976)
15. E.L. Uzunova, I.G. Mitov, D.G. Klissurski, Bull. Chem. Soc. Jpn **70**, 1985 (1997)
16. Y. Waseda, K. Shinoda, K. Sugiyama, Z. Naturforsch. A **50**, 1199 (1995)
17. S. Ayyappan, J. Philip, B. Raj, J. Phys. Chem. C **113**, 590 (2009)
18. Z. Wang, P. Lazor, S.K. Saxena, H.S.C. O'Neill, Mater. Res. Bull. **37**, 1589 (2002)
19. P.R. Graves, C. Johnston, J.J. Campaniello, Mater. Res. Bull. **23**, 1651 (1988)
20. P. Chandramohan, M.P. Srinivasan, S. Velmurugan, S.V. Narasimhan, J. Solid State Chem. **184** 89 (2011)
21. A. Franco, Jr., F.C.E. Silva, Appl. Phys. Lett. **96**, 172505 (2010)
22. C. Kittel, *Introduction to Solid State Physics*, 3rd edn. (John Wiley & Sons, New York, 1967)
23. N.W. Ashcroft, N.D. Mermin, *Solid State Physics* (Saunders College Publishing, Philadelphia, 1976)
24. H. Zeng, J. Li, J.P. Liu, Z.L. Wang, S. Sun, Nature **420**, 395 (2002)